3D Printing of solvent-free PEO-Polyolefin solid polymer electrolyte by Fused Filament Fabrication

Félix Bourseau, Sylvie Grugeon, Ugo Lafont, Loïc Dupont

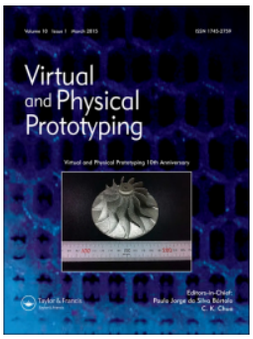

Virtual and Physical Prototyping

ISSN: (Print) (Online) Journal homepage: www.tandfonline.com/journals/nvpp20

3D Printing of solvent-free PEO-Polyolefin solid polymer electrolyte by Fused Filament Fabrication

Félix Bourseau, Sylvie Grugeon, Ugo Lafont & Loïc Dupont

To cite this article: Félix Bourseau, Sylvie Grugeon, Ugo Lafont & Loïc Dupont (2024) 3D Printing of solvent-free PEO-Polyolefin solid polymer electrolyte by Fused Filament Fabrication, Virtual and Physical Prototyping, 19:1, e2409975, DOI: 10.1080/17452759.2024.2409975

To link to this article: https://doi.org/10.1080/17452759.2024.2409975

VIRTUAL AND PHYSICAL PROTOTYPING
2024, VOL. 19, NO. 1, e2409975 (12 pages)
https://doi.org/10.1080/17452759.2024.2409975

Taylor & Francis
Taylor & Francis Group

3D Printing of solvent-free PEO-Polyolefin solid polymer electrolyte by Fused Filament Fabrication

Félix Bourseau[a,b], Sylvie Grugeon[a,b], Ugo Lafont[c] and Loïc Dupont[a,b,d]

[a]Laboratoire de Réactivité et de Chimie des Solides, UMR CNRS 7314, Hub de l'Energie, Université de Picardie Jules Verne, Amiens, France; [b]Réseau sur le Stockage Electrochimique de l'Energie (RS2E), FR CNRS 3459, Hub de l'Energie, Amiens, France; [c]European Space Research & Technology Centre, Noordwijk, The Netherlands; [d]Plateforme de Microscopie Electronique (PME) de l'Université de Picardie Jules Verne, Hub de l'Energie, Amiens, France

ABSTRACT

3D printing of energy storage systems is at the heart of In-Space Manufacturing strategy. Within this context, Li-ion polymer batteries printing through Fused Filament Fabrication (FFF) is envisaged. This study is devoted to optimising the extruded solid polymer electrolyte filament properties. As the poly(ethylene oxide) (PEO) – lithium bis(trifluoromethanesulfonyl)imide (LiTFSI) electrolyte offers the best Li^+ conductivities but suffers from poor mechanical behaviour, poly(propylene) (PP) is added to ensure filament printability. An exhaustive investigation highlights the impact of the PEO molar weight and the LiTFSI and PP proportions. Fine-tuning these parameters alters molten phase viscosity, which affects the electrolyte morphology and ionic conductivity. Best formulations feature a co-continuous structure that provides effective mechanical reinforcement and exhibits the best ionic conductivity reported so far for an FFF-printed solvent-free polymer electrolyte of 1.2×10^{-4} S.cm^{-1} at 70°C. Therefore, it opens the way towards polymer battery printing, on the Earth and in microgravity conditions.

ARTICLE HISTORY
Received 31 July 2024
Accepted 21 September 2024

KEYWORDS
3D printing; FFF; polymer electrolytes; Li-ion batteries; In-Space Manufacturing; solvent-free

Introduction

On the way to Mars, space agencies are preparing human come-back on the Moon, for a durable occupation through the Artemis programme [1]. In Space, an astronaut's life mainly relies on the resupplies from the Earth: 3 days to reach the moon and 2 billion dollars per launch for the Space Launch System developed by NASA [2]. Even if the economic and environmental costs of rocket launches are decreasing, it is impossible to consider the future of space exploration with this model. Therefore, In-Space Manufacturing (ISM) is a key approach that involves the development of versatile tools to enable out-of-earth manufacturing of devices such as spare parts, energy production systems, or foods [3]. It could reduce the need for resupplies, decrease the storage of spare parts by 78% in mass [4], and offer new capabilities by removing constraints from space systems design linked to rocket launch. Additive manufacturing (AM) is at the heart of this strategy as it allows for the production of low-volume and low-cost customisable 3D shapes, with various materials. Among additive techniques, Fused Filament Fabrication (FFF) has been successfully deployed in the ISS to 3D print spare parts and tools [5, 6]. Today, in-orbit 3D printing of more complex systems with added functionalities is the next challenge to take up. As Energy is the foundation stone of every operating system, manufacturing of energy production and storage devices in microgravity is a necessary milestone to carry out the ISM transition. Within this context, in-space 3D printing of batteries would be a key achievement.

On Earth, 3D printing recently appeared as a new manufacturing process for energy storage devices [7, 8]. It paves the way for 3D-designed electrodes and batteries resulting in improving the electrochemically active surface, power, and specific capacity meanwhile reducing dead volume and dead weight [9–12]. The growing need for micro-batteries and customisable devices also contributes to the outbreak of AM in battery manufacturing [13]. Several AM techniques

CONTACT Loïc Dupont loic.dupont@u-picardie.fr Laboratoire de Réactivité et de Chimie des Solides, UMR CNRS 7314, Hub de l'Energie, Université de Picardie Jules Verne, 15 rue Baudelocque, Amiens 80039, France; Réseau sur le Stockage Electrochimique de l'Energie (RS2E), FR CNRS 3459, Hub de l'Energie, 15 rue Baudelocque, Amiens 80039, France; Plateforme de Microscopie Electronique (PME) de l'Université de Picardie Jules Verne, Hub de l'Energie, Amiens 80000, France

Supplemental data for this article can be accessed online at https://doi.org/10.1080/17452759.2024.2409975.

offer the possibility to achieve multi-material printing, necessary to obtain entire batteries [14]. Among them, material extrusion [15] and more specially FFF have been investigated to manufacture Li-ion batteries because this is one of the cheapest, easiest, and most versatile methods. FFF 3D printing of batteries relies on the use of composite filaments, made of a thermoplastic polymer matrix loaded with active and conductive materials. Significant progress has been gradually made in formulating suitable filaments for electrodes and separators: from low-loaded polylactic acid (PLA) [16–18] to architecturally engineered electrodes providing promising performances [19]. However, in these studies, liquid electrolytes are still used to soak 3D-printed separators. Thus, polymer electrolyte printing is the last step to manufacture entire Li-ion batteries through a one-step solvent-free process (Figure S1). Such a process is mandatory for 3D printing without gravity and to fit spacecraft safety requirements.

Polymer electrolytes have been deeply studied for their interface properties with metallic lithium but still present low ionic conductivity at room temperatures (10^{-8}-10^{-5} S.cm^{-1} at 25°C). They also possess poor rigidity and mechanical resistance making their 3D printability difficult. That is why, only two studies have been reported so far on Solid Polymer Electrolyte (SPE) printing by FFF. Maurel *et al.* [20] have tried to print poly(ethylene oxide) (PEO)/ lithium bis (trifluoromethanesulfonyl)imide (LiTFSI) SPE composed of PEO Mn∼100,000 and PEO Mn∼5,000,000 in 90:10 wt%, with a molar ratio O/Li$^+$ = 20:1. This system has been extensively reported as the most ionic conductive polymer/Li salt couple in temperature, due to the high segmental mobility and the convenient donor number of PEO [21, 22]. However, the lack of rigidity and the sticky behaviour of pure PEO/LiTFSI strongly hinder its printability. Thus, they have modified a classical 3D printer and succeeded in 3D printing a SPE having an ionic conductivity of 2.2×10^{-3} S.cm^{-1} at 90 °C and 4.9×10^{-6} S.cm^{-1} at 30 °C. At the same time, Ragones *et al*. have obtained a lower ionic conductivity (3×10^{-5} S.cm^{-1} at 90°C) but a better printability for their SPE composed of PLA, PEO, LiTFSI, and SiO_2 (59:20:20:1 wt.%) [23]. More recently, they reached an ionic conductivity of 2×10^{-4} S.cm^{-1} at 60°C in a quasi-solid printed electrolyte soaked by LiTFSI ionic liquid [24]. Therefore, new strategies have to be found to improve the 3D printability without degrading electrolyte performances. In our previous work, polymer-based electrolyte strategies have been reviewed to identify the most suitable methods for SPE 3D printing by FFF [25]. Among them, immiscible polymer blending and composite polymer electrolyte (CPE) appear to be promising strategies that are compatible with ISM requirements.

Thus, considering the first strategy, we embarked on the development and characterisation of a novel 3D-printed polymer electrolyte based on an immiscible blend of polymers. Poly(propylene) (PP) was chosen as the mechanical phase, and PEO coupled with LiTFSI as the ionic conductive phase. First, we undertook an exhaustive experimental study to understand the effect of polymer mass ratio (PEO:PP wt%), Li salt content (O/Li$^+$), and polymer molar weight (PEO M_w∼10^5:PEO M_w∼5×10^6 wt%) on the ionic conductivity. The impact of these parameters on the morphology has been highlighted due to modifications of the volume fraction and viscosity ratio [26]. Electrolyte architecture was carefully studied and linked to conductivity properties through Differential Scanning Calorimetry (DSC), Electrochemical Impedance Spectroscopy (EIS), and Scanning Electron microscopy (SEM). In the second part, we optimised the formulation to obtain a polymer electrolyte filament 3D printable on a commercial device. After 3D printability trials, EIS and SEM analysis combined with electrochemical tests were achieved on 3D printed disks of electrolyte.

Experimental section

Materials

Poly(ethylene oxide) (PEO) M_w∼100,000 (referred to as PEO100 K) (d_{peo} = 1.23) and M_w∼5,000,000 (referred to as PEO5M) (d_{peo} = 1.23) powders were supplied by Alfa Aesar and used as received. Ultrasint nat 01 poly(propylene) (PP) powder (d_{pp} = 0.91) was supplied by BASF 3D Printing Solutions GmbH, Germany. This polymer has a lower melting point compared to a common PP (T_m = 140°C vs. T_m = 170°C), which allows processability in the same range of temperatures as PEO. $LiFePO_4$ (LFP, pulverised morphology type, particle size D50: 2–6 µm, 11–15 m^2 g^{-1}, carbon content: 1.3–1.6%) was kindly provided by the company Aleees, Taiwan. C45 conductive carbon (45 m^2/g) was purchased from Imerys. Lithium bis(trifluoromethanesulfonyl)imide (LiTFSI) powder was purchased from Solvionic, France. LiTFSI was stored in a glove box and transferred for experiments in a dry room. All of the materials were hereafter manipulated in a dry room (dew point ⩽ −45 °C). The absence of water has been checked by Fourier transform IR; no extra pics were visible in the 3500 cm^{-1} regions (Figure S2 of the supplementary material).

Filament extrusion

The filament extrusion was carried out in the dry room using a Haake Minilab 3, twin-screw extruder (Thermofisher Scientific, USA) which was fed with premixed dry

powders. The extruder was used in co-rotating mode with two extrusion dies: a rectangular shape (5 mm x 0.5 mm) to extrude films and a cylindrical shape to produce ~a 1.75 mm diameter filament for 3D printing. Screw rotation was fixed at 50 RPM, the temperature was fixed typically at 170 °C for PP-containing samples and 85°C for those without PP to avoid as much as possible PEO degradations. The filament coming out from the extruder nozzle was received by an M22 transport conveyor (Thermofisher Scientific, USA). Prior extrusion of each sample, the extruder was cleaned thoroughly with neat poly(styrene).

Electrochemical Impedance Spectroscopy (EIS).

An MTZ-35 frequency response analyzer and an Intermediate Temperature System (ITS) developed by Bio-Logic, France, were used to perform the Electrochemical Impedance Spectroscopy (EIS) analysis. In the dry room, samples were sandwiched between 6.35 mm diameter gold electrodes placed in an enhanced controlled environment sample holder (CESH-e) provided by Biologic. This cell enables the application of a constant force of 6N on the samples, as well as allows users to acquire sample thicknesses before and after the measurement. Beforehand, the sample underwent a first heating step at 100 °C for 30 min to improve the contact with electrodes and avoid thickness variation due to the melting of some samples. Subsequently, AC impedance measurements were performed at various stabilised temperatures ranging from 20 °C to 90 °C (ramp rate of 1.0 °C min^{-1}, stabilisation time before measure of 15 min) in a frequency range of 30 MHz to 0.1 Hz (20 points per decade and 10 measures per point) and at an excitation voltage of 0.05 V. Measurements of thickness were performed on the sample holder before and after the acquisition to take into account the thickness variation in ionic conductivity calculation. Through-plane ionic conductivities were calculated from the following equation:

$$\sigma = \frac{1}{R} \times \frac{d}{A}$$

where d is the sample thickness, A is the sample surface area, and R is the respective resistance deduced from the Nyquist and Bode plots. Note that the ionic conductivity values were taken perpendicularly to the printing and extrusion direction which is the most unfavourable case.

Scanning electron microscopy (SEM)

The microstructure of films and SPE filaments was investigated using a FEI Quanta200F (Thermo Fisher Scientific, USA) scanning electron microscope under high vacuum. The secondary electron images were recorded with a 10 keV electron beam acceleration voltage with a magnification of x 400 and x 300, at a working distance of 10 mm. In a dry room, samples were cut into liquid nitrogen to perform cross-sectional observation.

3D printing

3D printing of the filaments in the form of 16 mm diameter and 0.2 mm thick discs was carried out using the Original Prusa i3 MK3 3D printer. The disc was designed using Autodesk® Fusion 360 software and sliced to print specifications using PrusaSlicer 2.5.0 software. The outlet nozzle diameter was 0.4 mm. Printing parameters such as print speed and nozzle and bed temperatures were tuned to 18 mm s^{-1}, 220 C, and 70 °C, respectively. Before each printing, the printer was purged with PLA and a first layer calibration was performed to adjust the nozzle positioning. The filament diameter was controlled to be 1.75 mm. The pressure of the rolling by the screw was maintained at the same level between printing.

Electrochemical measurements

Coin cells were assembled in a dry room (dew point $\leqslant$ −45 °C). A blend of PEO (M_w~10^5)/LFP/C45 (40:50:10 wt%) solvent-cast onto a stainless steel disc was used as a working electrode and metallic lithium as a reference and counter electrode. For the PEO reference electrolyte membrane, two layers of 160 µm have been stacked and for printed electrolyte, only one layer was used with a thickness between 230–250 µm. After assembling, cells were subjected to a resting time of 5 h then a cycling protocol in galvanostatic mode at 80 °C and at 40 °C, at the following rates: 5 cycles at C/20, C/10, C/5, then C/20, in the voltage range of 3–3.6 V (*vs.* Li/Li^+). Symmetric coin cells Li^0/Li^0 were assembled with 230–250 µm thick printed electrolytes. Successive current densities were applied by steps of a minimum 6 cycles of 2 h. The polarisation recorded was an average of the voltage obtained during each step. All cells were cycled inside the oven 9010–0153 FP (Binder GmbH, Germany), using the galvanostat BCS-805 (Bio-Logic, France).

Results and discussion

Effect of key parameters on the ionic conductivity

The influence of the polymer mass ratio (PEO: PP wt%), the Li salt content (O/Li^+), and the PEO molar weight

(PEO $M_w \sim 10^5$: PEO $M_w \sim 5 \times 10^6$ wt%) on the ionic conductivity of solid polymer electrolytes has been studied on extruded film pieces. All sample compositions are summarised in Figure S3 of the supplementary material.

Effect of the PEO:PP mass ratio **–** The influence of increasing PP content was studied at six different PEO (Mn∼100,000):PP weight ratios: 100:0, 80:20, 70:30, 60:40, 50:50, 40:60; with a constant loading in LiTFSI following the molar ratio $O/Li^+ = 20:1$. Two possible competing effects were reported in the literature: an increase in ionic conductivity by reducing PEO crystallinity, and a decrease in ionic conductivity induced by a rise in conducting phase tortuosity [27]. Arrhenius plots acquired by EIS are depicted in Figure 1, with pure PEO/LiTFSI 20:1 solvent cast membrane as a reference established by Maurel *et al*. [20].

Above the PEO melting point ($T_m = 50$ °C), lower ionic conductivities are obtained with the addition of PP. At these temperatures, PEO is fully amorphous and the ionic conductivity drop can be explained by the rise in inactive material inside the electrolyte increasing the tortuosity (Figure 1). Bouchet *et al*. [29], have successfully described the conduction properties of their block copolymer electrolyte PEO-PS, thanks to the Carman model which links the ionic conductivity and the tortuosity. They validated their model by fitting the assumed Weissberg expression which describes the tortuosity as a function of the conductive volume fraction (Table 1). The same method has been applied in this work, to highlight the link between the tortuosity induced by PP, and the ionic conductivity. Figure 2 displays tortuosity values calculated with the Carman relation from EIS measurements. Two behaviours can be distinguished for points above 50 °C. For PP content below 40 wt%, the points in the low tortuosity zone (Figure 2) fit the Weissberg's model for $p = 1$. Indeed, PP domains stay discontinuous, so the tortuosity slowly increases with the addition of PP following the probabilistic approach developed by Weissberg. PP inclusions are visible in the PEO + LiTFSI matrix on SEM images as agreed with the low tortuosity (Figure 2). For PP content above 40 wt% (point in the high tortuosity zone (Figure 2)), the tortuosity sharply increases and no longer fits Weissberg's model. SEM pictures clearly show the coalescence of PP nodules that progressively increases the tortuosity and reduces the continuity of the conductive phase.

Below the PEO melting point, PP-containing samples show higher ionic conductivity than pure PEO/LiTFSI (Figure 1). As revealed by DSC measurements, PP disturbs the rearrangement of the PEO chains thus decreasing its crystallinity (Figure 1). A larger amount of PEO amorphous phase enabling the chain segmental mobility leads to higher bulk ionic conductivity (σ_0) in Table 1. It explains uncoherent low values of tortuosity calculated by the Carman model (points in the semi-crystalline zone in Figure 2). Thus, the ionic conductivity is slightly improved with 20 wt% of PP because the crystallinity is disturbed without a huge increase in tortuosity. From 20 to 50 wt%, the ionic conductivity is decreased because the effect of tortuosity is stronger than the crystallinity reduction effect. PEO is still semi-crystalline at 41-43% as agreed with the change of slop in Arrhenius plots in Figure 1, and the strong recrystallization peak on the DSC curve (Figure S4 of the supplementary material). Finally, at 60 wt% of PP, there is no change of slopes because PP strongly reduces PEO crystallization down to 18.2%. Thus, the addition of PP helps to disturb the PEO crystallinity, but it must be limited to maintain a low tortuosity to avoid important ionic conductivity loss.

Effect of Li salt content **–** The effect of lithium salt was investigated at different O/Li^+ molar ratios 20:1, 15:1, 10:1, 8:1, 5:1 in SPE with PEO:P*P* = 50:50 wt% and PEO100K:PEO5M = 50:50 wt%. Below the PEO melting point, there is a rise in conductivity from $O/Li^+ =$ 20:1 to $O/Li^+ =$ 10:1. According to DSC analyses, this result is correlated with a strong decrease of PEO crystallinity till a full amorphous PEO phase at room temperature for $O/Li^+ = 10:1$ (Figure 3). As reported in the literature, this ratio gives the best ionic conductivity, because higher Li salt contents favour ion pairing, which acts as a barrier for Li^+ motion reducing the overall conductivity [20]. Above the PEO melting point, the PEO is fully amorphous so the ionic conductivity should decrease from $O/Li^+ = 20:1$ to $O/Li^+ = 5:1$ as demonstrated by Maurel *et al.* on pure PEO/LiTFSI electrolytes [20]. However, EIS results still display the best ionic conductivity for $O/Li^+ = 10:1$ at high temperatures proving the existence of an additional effect (Figure 3). In equivalent proportion between PEO and PP, the less viscous phase tends to be continuous whereas the other one forms droplets. Increasing LiTFSI reduces the PEO/LiTFSI viscosity (plasticising effect), and makes its structure more continuous with less tortuous pathways for Li^+ so better ionic conductivity. SEM images corroborate this statement: there are PEO droplets (in white) in a matrix of PP (in black) for a low LiTFSI content ($O/Li^+ = 20:1$) whereas PEO starts to become continuous for a higher LiTFSI content ($O/Li^+ = 10:1$) (Figure S6 of the supplementary material). $O/Li^+ = 8:1$ and 5:1 still have lower ionic conductivities because the ion pairing effect is stronger than the morphological effect.

Effect of PEO molar weight – The effect of the PEO chain length was studied through the various PEO100K:PEO5M weight ratios of 100:0, 75:25, 50:50, and 0:100, in SPE with PEO:P*P* = 50:50 wt% and $O/Li^+ =$

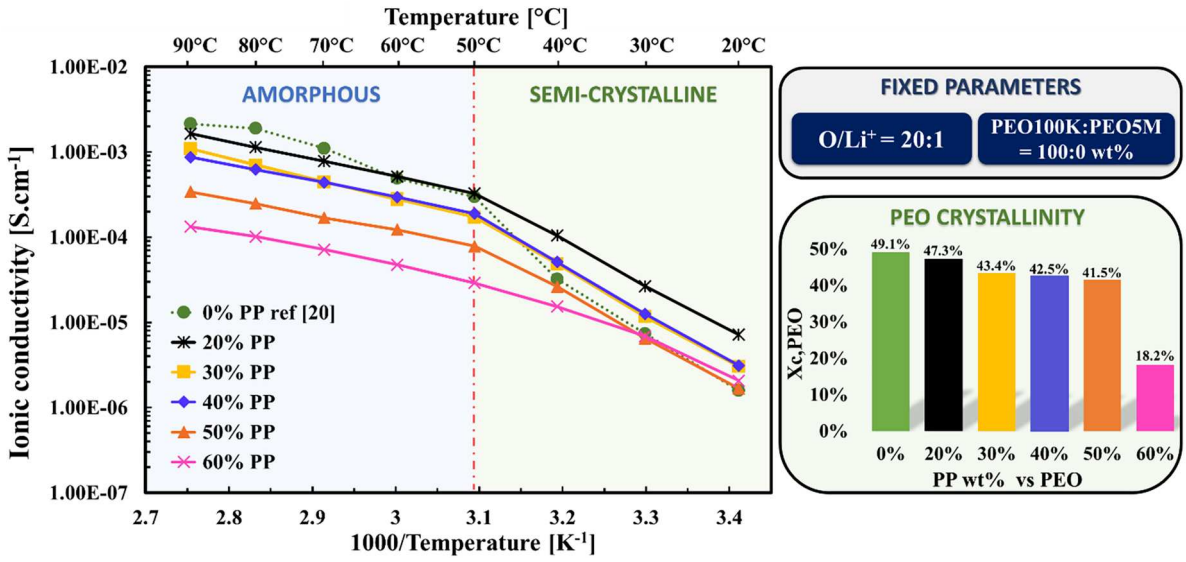

Figure 1. Arrhenius plot of ionic conductivity for several PEO: PP wt% ratio (100:0, 80:20, 70:30, 60:40, 50:50, 40:60) in SPE with PEO100K:PEO5M = 50:50 wt% and O/Li^+ = 20:1, as function of temperature (expressed in 1000/T [K^{-1}] for the bottom axis and T [°C] for the top axis), and PEO crystallinity measurements from DSC curves (Figure S4 of the supplementary material), with $\Delta H_{fus,\ 100\%\ crystalline} = 194.6\ J.g^{-1}$ [24, 28].

20:1. According to the literature, these two PEOs have too long chains to influence the ionic conductivity via a vehicular mechanism (diffusion of Li^+-coordinated chains) [30]. However, Arrhenius plots acquired by EIS show a diminution of the ionic conductivity along with higher PEO molar weight (Figure 4). In the same way as for LiTFSI, PEO chain length modifications affect its viscosity and therefore the morphology of the blend. Higher PEO molar weight induces higher PEO + LiTFSI viscosity, which reduces its continuity so restricting Li^+ conduction. For low PEO molar weight ratios (100:0 and 75:25), The PEO + LiTFSI viscosity is sufficiently low to obtain a continuous conductive matrix (light PEO + LiTFSI matrix in SEM pictures). The small gap of ionic conductivity between 100:0 and 75:25 ratio is explained by the increase of PEO + LiTFSI tortuosity. For high molar weight PEO ratios (50:50 and 0:100), the conductive phase forms droplets that hinder efficient Li^+ motion. The phase inversion from a PEO + LiTFSI matrix to a PP matrix, due to the higher viscosity of the PEO phase compared with PP (Figure S7 of the supplementary material), is visible in SEM images between the 75:25 and 50:50 weight ratios (Figure 4). It explains the differences in ionic conductivity between the low (100:0 and 75:25) and high ratios (50:50 and 0:100).

Table 1. (a) Carman Model (b) Weissberg theory.

Equation 1: Carman model	Equation 2: Weissberg's theory	
$\sigma = \frac{\sigma_0 \varepsilon}{\tau}$	$\tau = 1 - p \times \ln(\varepsilon)$	*σ: Ionic conductivity of the electrolyte* *σ_0: Ionic conductivity of the conductive phase* *ε*: Volume fraction of the conductive phase *τ: Tortuosity of the conducting phase* *p: Parameter of the model*

Fine-tuning PEO mass fractions and viscosities to obtain a co-continuous morphology – As demonstrated, SPE morphology, influenced by the three aforementioned parameters, has a huge impact on ionic conductivity because the PP phase is not involved in Li^+ conduction. Continuity of the conductive phase (PEO + LiTFSI), with as low tortuosity as possible is necessary to obtain efficient pathways for Li^+. However, the continuity of the mechanical phase (PP) is also targeted to ensure enough mechanical reinforcement for the 3D printing. Thus, conditions to obtain a co-continuous morphology with low tortuosity have been studied. Potschke *et al.* [26] have reviewed existing empirical models (fine dotted lines in Figure 5) which describe co-continuity conditions for an immiscible extruded polymer blend, depending on the viscosity ratio and the volume fraction of each phase. In our study, conductive phase viscosity is influenced by the plasticising effect of LiTFSI and the PEO molar weight, whereas volume fraction is linked to the PEO:PP weight ratio. The viscosity of several extruded samples of different formulations has been investigated to place them on the morphology diagram, and SEM observations were performed to determine the cross-sectional continuity of each phase (Figure 5). Formulations in green are composed of a PEO/LiTFSI matrix with entrapped droplets of PP. In this region, the low tortuosity does not decrease the global ionic

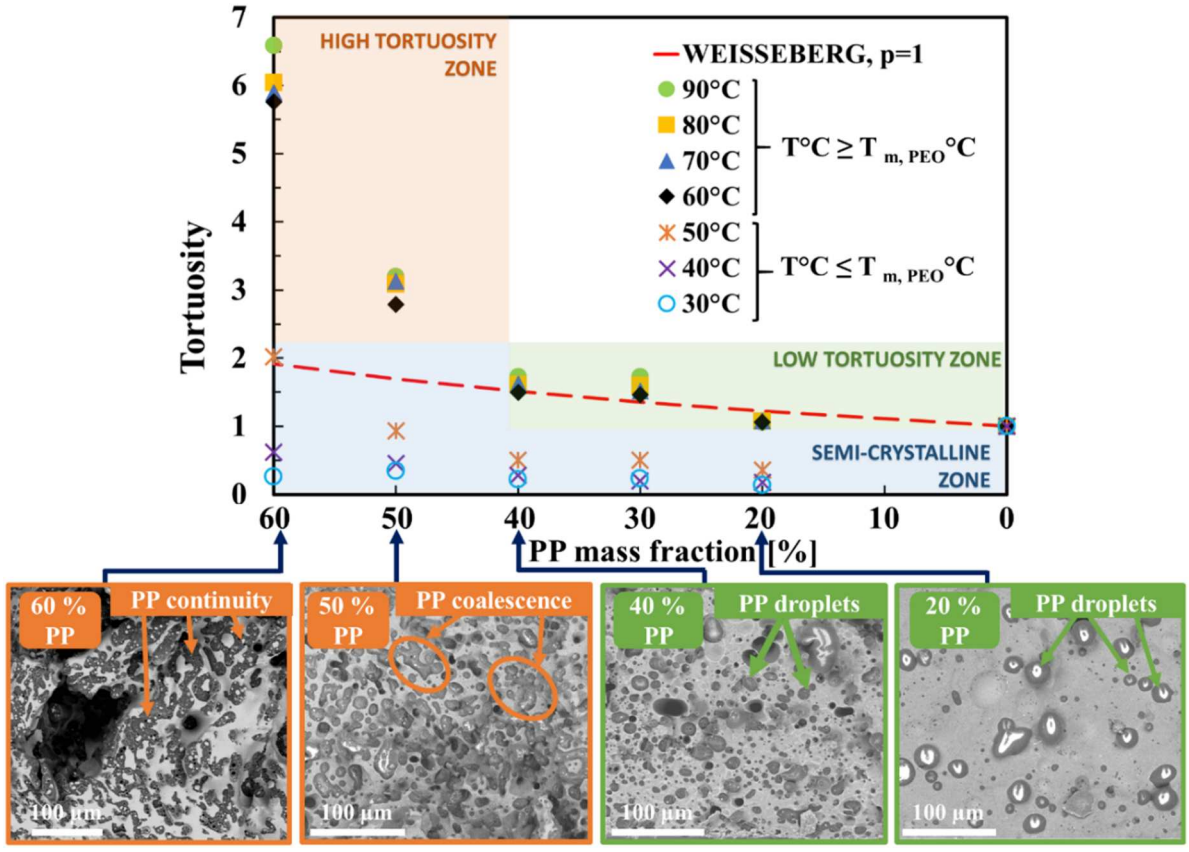

Figure 2. Tortuosity calculated with the Carman model (ionic conductivity measured by EIS) and Weissberg theoretical model. Results are coupled with cross-section SEM images in Back Scattered Electron (BSE) mode, (white: PEO + LiTFSI, black: PP confirmed by EDS (Figure S5 of the supplementary material)).

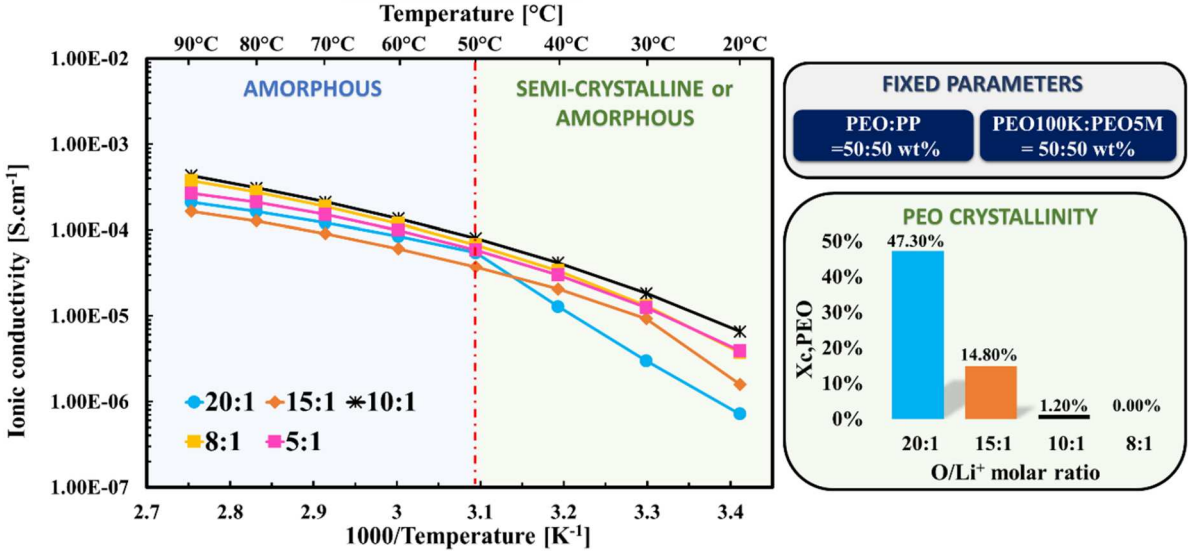

Figure 3. Arrhenius plot of ionic conductivity for several O/Li^+ molar ratios (20:1, 15:1, 10:1, 8:1, 5:1) in SPE with PEO:P*P* = 50:50 wt% and PEO100K:PEO5M = 50:50 wt%, as function of temperature (expressed in 1000/T [K^{-1}] for the bottom axis and T [°C] for the top axis), and PEO crystallinity measurements from DSC curves (Figure S4 of the supplementary material), with $\Delta H_{fus,\ 100\%\ crystalline} = 194.6\ J.g^{-1}$ [24, 28].

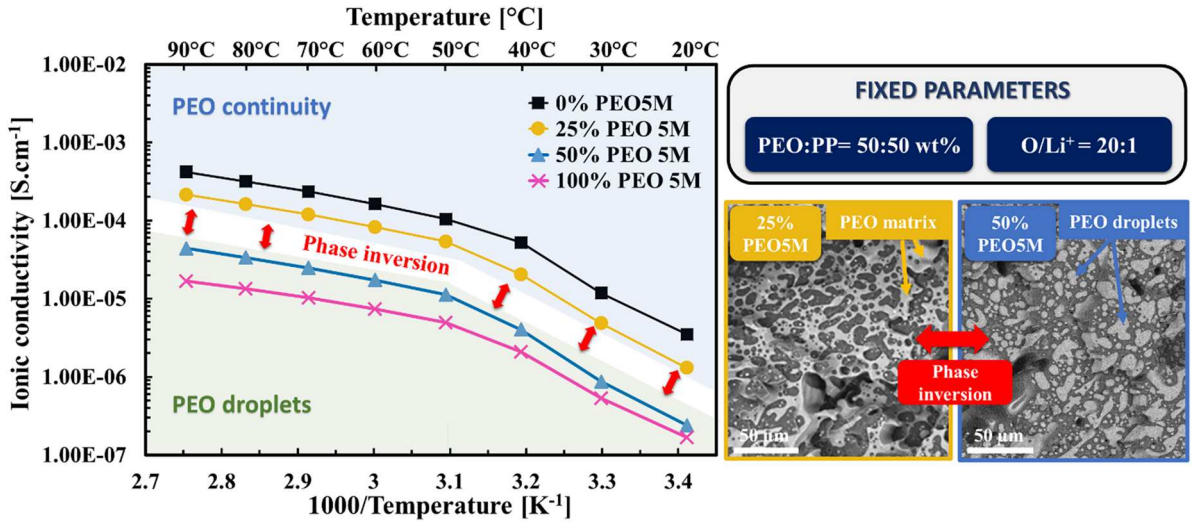

Figure 4. Arrhenius plot of ionic conductivity for several PEO molar weight % ratio (PEO100K:PEO5M = 100:0, 75:25, 50:50, 0:100) in SPE with PEO:P*P* = 50:50 wt% and O/Li^+ = 20:1, as function of temperature (expressed in 1000/T [K^{-1}] for the bottom axis and T [°C] for the top axis), coupled with cross-section SEM images, BSE, 10 kV, x300.

conductivity. On the opposite side, in blue, the conductive phase is entrapped in the PP matrix which is harmful for the ionic conductivity. Between these two regions, SEM pictures showcase targeted co-continuous structures between PEO and PP. If PEO + LiTFSI viscosity is lower than PP viscosity, co-continuity is obtained for low content of PEO. Conversely, if PP viscosity is lower, co-continuity is obtained for a high content of PEO. It gives a linear domain in orange favourable to co-continuity formation with our process parameters (T = 170° C, 50 RPM, residence time = 10 min). SEM pictures for all the points are summarised in Figure S8 of the supplementary material.

All aforementioned effects of the three studied parameters on the global ionic conductivity can be explained with the Carman model. An increase in the LiTFSI and PP proportion has a positive impact on the bulk ionic conductivity (σ_0) through conductive phase crystallinity decrease and cation concentration modification. Besides, the three parameters have interdependent effects on the blend morphology which must be tuned to ensure co-continuity.

Formulation optimisation toward FFF 3D printing

The effects of the above parameters on the polymer electrolyte conductivity have been deeply investigated. However, improving the ionic conductivity is in conflict with improving the printability. That is why optimisation of filament formulation has been performed to manage to 3D print a polymer electrolyte using FFF. In this part, all electrolyte samples have been characterised on printed disks. The different compositions are summarised in Figure S9 of the supplementary material.

Electrolyte 3D printing – Starting from the ideal formulation in terms of ionic conductivity at 25°C as determined in the first part, the aim was to modify parameters until obtaining a 3D printable electrolyte with a commercial set-up. To evaluate the printability, various samples have been extruded under the shape of 1.75 mm of diameter filaments to feed a Prusa 3D printer with a 0.4 mm nozzle. A filament was considered 3D printable if a one-layer thick disk (200 µm) (Figure 6e and f) could have been successfully printed on this set-up several times following a test procedure (Figure S10 of the supplementary material). Figure 6 displays the design of the experiments to optimise the formulation. The four PEO:PP polymer weight ratios, 80:20, 70:30, 60:40, and 50:50, where PEO is mainly continuous, have been investigated. Four O/Li^+ ratios from 20:1–8:1 and various contents of PEO molar weight were also tested. Red cases symbolise non-printable formulations whereas green ones symbolise formulations suitable for 3D printing. In the case of a non-printable sample, four main defaults happen; filament buckling before the feeding head (Figure 6b and c), filament crushing (Figure 6a) inside the printing head, filament breaking inside the Teflon tube (Figure 6d), and nozzle clogging due to a sticky behaviour.

Formulations with PEO:PP weight ratios equal to 80:20 and 50:50 have been discarded. Indeed, 20 wt% of PP is not sufficient to strengthen the mechanical behaviour, leading to non-3D printable filament whatever the O/Li^+ ratios and PEO molar weights.

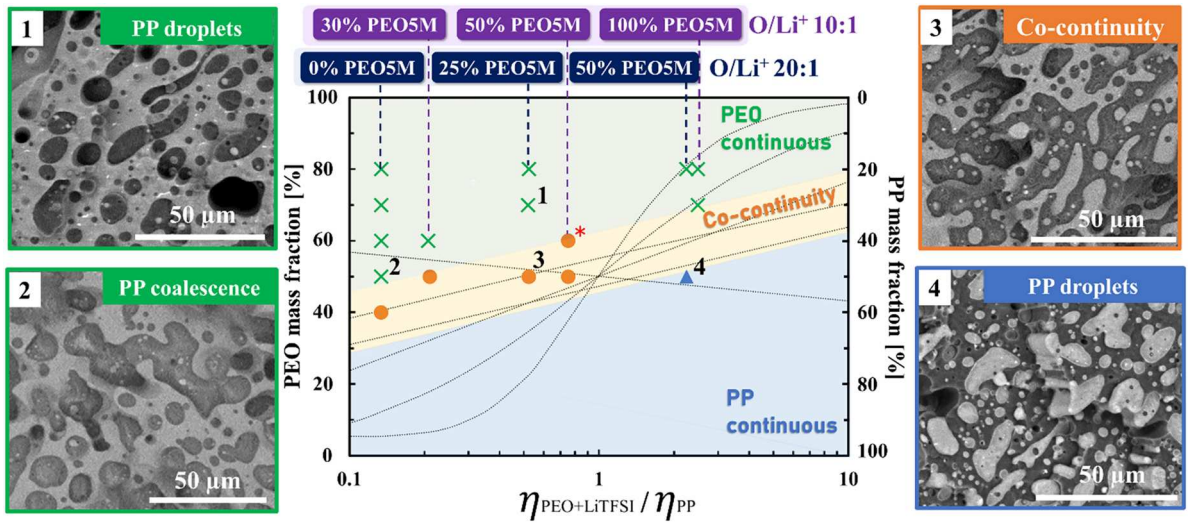

Figure 5. PEO wt% (can be approximated as volume% due to close densities) vs. viscosity ratio diagram highlighting three types of morphology: PEO continuity (green), co-continuity (orange), and PP continuity (blue), illustrated by cross-section SEM images, BSE, 10 kV, x300 SEM images. Fine black dotes lines represent all the empirical models describing the co-continuity of polymer immiscible blends mentioned in [26].

Filaments lack stiffness due to the absence of PP continuity and present a sticky behaviour due to the huge amount of PEO + LiTFSI. Conversely, 50 wt% of PP gives enough mechanical reinforcement to 3D print the electrolyte with all O/Li^+ ratios and PEO molar weights. However, such high PP wt% induces a high tortuosity for all samples thus limiting the ionic conductivity at 5.9×10^{-6} $S.cm^{-1}$ at 25°C for the best formulation ($O/Li^+ = 8:1$ and 60 wt% of PEO5M) as described previously.

For 30 and 40 wt% of PP, filament printability depends on the amount of lithium salt and the molar weight of PEO. 30 wt% PP only permits printing of lightly-loaded in Li salt filaments (maximal $O/Li^+ = 15:1$). A filament has been successfully printed with $O/Li^+ = 15:1$ and at least 60% PEO5M in the PEO matrix, giving the best ionic conductivity at 75°C (3.3×10^{-4} $S.cm^{-1}$). However, it gives a lower one (5.7×10^{-6} $S.cm^{-1}$) at 30°C because the PEO is still semi-crystalline in these conditions. Moreover, this formulation would not be in the co-continuous zone (Figure 5), explaining a lack of reproducibility during the printing. Thus, the best compromise was found for 40 wt% of PP, which permits to reach printability with the optimal ratio of

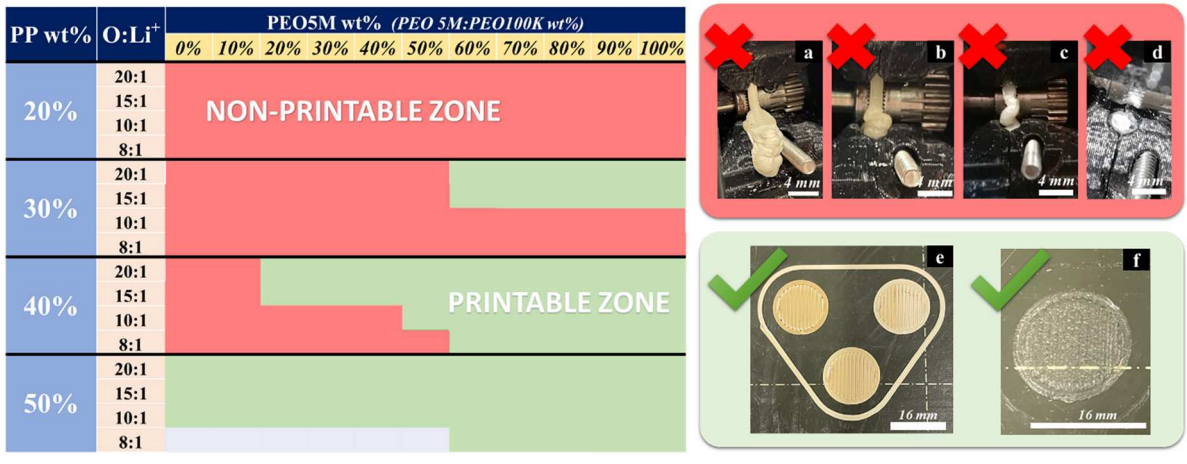

Figure 6. Printability tests and experimental design according to the three main parameters. Examples of failed printing tests are illustrated with inside pictures of the 3D printer (above the heating block figure (S10)): (a) Filament crushing by the rolls linked to a soft and sticky behaviour, (b and c) filament bending linked to a lack of stiffness, (d) filament breaking and blocking inside the Teflon tube of the printer linked to a lack of flexibility. Successful tests are illustrated by 200 µm thick printed disks of polymer electrolyte without under extrusion (e and f).

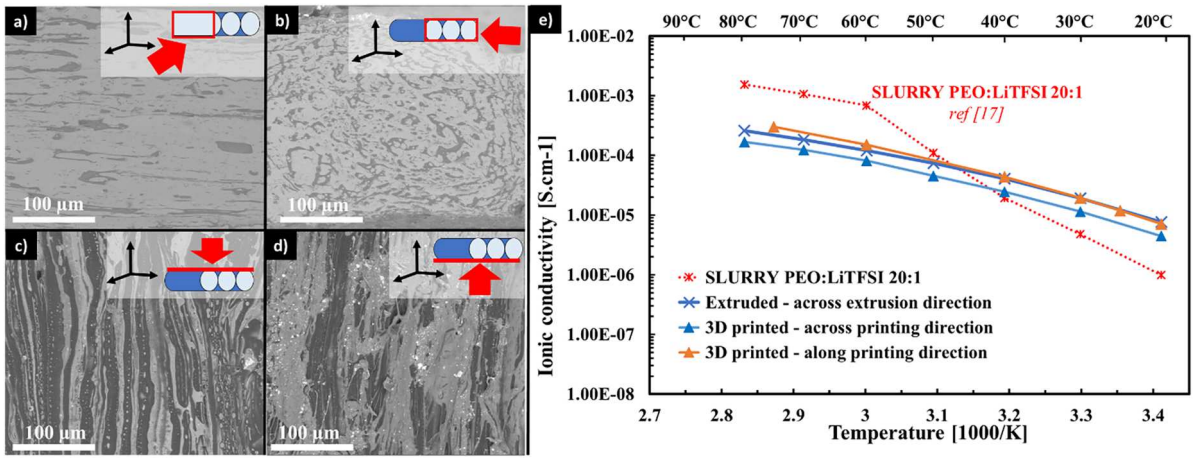

Figure 7. SEM of the printed optimised electrolyte formulation (PEO:PP 60:40 wt%, O/Li $^+$ 20:1, PEO100K:PEO5M 50:50 wt%). Cross sections (a) parallel to the printing direction, (b) perpendicular to the printing direction, (c) top surface, (d) bottom surface; (e) Arrhenius plots of the extruded optimised formulation, the same printed with different orientations, and the reference solvent cast membrane without PP.

$O/Li^+ = 10:1$. 50 wt% of heavier PEO is needed to counterbalance the LiTFSI plasticising effect and obtain a formulation located in the co-continuous area of the viscosity/volume fraction diagram (* on Figure 5). The electrolyte printed at 210°C with a bed temperature of 70°C provides an ionic conductivity of **1.5×10^{-5} S.cm^{-1} at 30°C** (Figure S11 of the supplementary material). This is the highest ionic conductivity at 30°C reported so far for a polymer electrolyte printed by FFF, even, this value still may be too low for Li-ion battery cycling at this temperature.

Optimised formulation characterisation – The best compromise between printing quality and ionic conductivity at 30°C was found for the polymer electrolyte formulation: PEO:P*P* = 60:40 wt%, PEO100K:PEO5M = 50:50 wt% and $O/Li^+ = 10:1$. SEM images on printed discs underline a co-continuous morphology made of PEO/LiTFSI and PP (Figure 7b). 3D printing acts as a second extrusion that homogenises the blend and induces anisotropic structures. Indeed, oriented thin domains of PP are visible along the printing direction (in dark in Figure 7a). Thus, the tortuosity of Li^+ pathways is lower along the direction of extrusion giving an improved ionic conductivity at all temperatures along the printing direction versus across the printing direction (Figure 7e). This is a key point to further consider for the 3D architecture of full-cell printing to improve their performance. In cross-section, printed electrolytes can be seen as an assembly of deposited strands (Figure S12 of the supplementary material). Inside the latter, the co-continuous domain structuring occurs concentrically on the outer edges of the deposited strands. This morphology

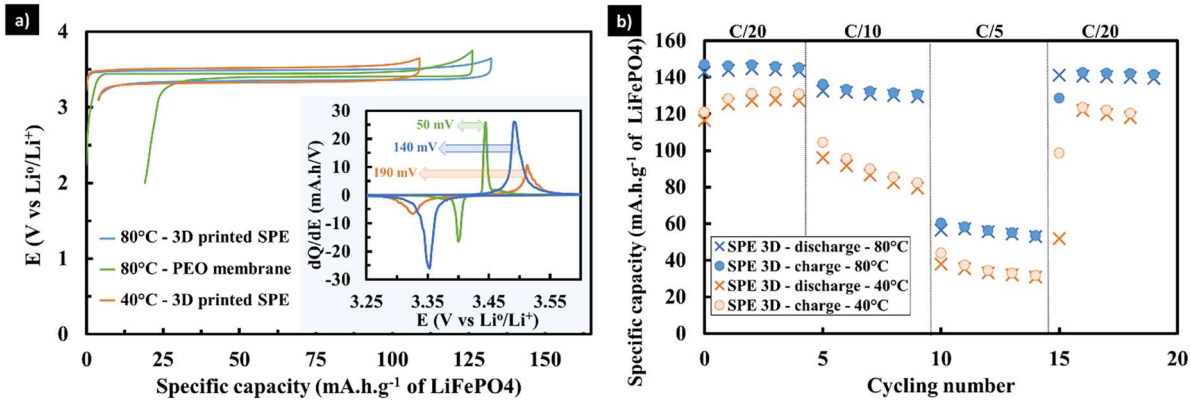

Figure 8. (a) 2nd Cycles at C/20 of the optimised printed electrolyte at 80°C (1.04 mAh/cm^2) and 40°C (0.53 mAh/cm^2), and a solvent cast membrane PEO-LiTFSI $O/Li^+ = 20:1$ at 80°C, in LFP/Li^0 cells with a polymer cathode membrane based on LFP/C45/PEO(M_w~10^5); with corresponding dQ/dE to quantify differences in polarisation (PEO membrane thickness = 320 µm and 3D printed electrolyte thickness = 230-250 µm); (b) Cycles of optimised printed electrolyte at 80°C and 40°C in LFP/Li^0 cells with the polymer cathode membrane

increases the tortuosity for Li^+ cross-sectional pathways which can explain the lower ionic conductivity for the 3D-printed electrolyte compared to extruded samples (Figure 7e). Finally, considering the gap in polymer melting temperatures (T_{PEO} = 50 °C vs T_{PP} = 140 °C), the printing temperatures (T_{nozzle} = 220 °C and T_{bed} = 70 °C) could have led to polymer phase segregation with the help of gravity. This is not the case because both phases are equally visible on the top (Figure 7c) and the bottom (Figure 7d) surfaces, confirming that the printing process does not induce inhomogeneities between the top and the bottom of the printed part.

Electrochemical tests – Beforehand, the best-printed polymer electrolyte (PEO:PP 60:40 wt%, O/Li^+ 20:1, PEO100K:PEO5M 50:50 wt%) has been tested in Li°||Li° symmetric coin cells at several temperatures and current densities to investigate polarisation (Figure S13). It enabled to assess of the maximal current densities to apply, and thus the appropriate theoretical areal capacity of the cathode in LFP/Li° cells. Afterward, this electrolyte/separator was inserted into a half-coin cell consisting of an LFP, C45, and PEO ($M_w \sim 10^5$) cathode solvent cast onto a stainless-steel disc and a lithium foil. Cells were successfully cycled at 80°C (1.04 mAh/cm^2) and 40°C (0.53 mAh/cm^2) and performances were compared with those of reference cells containing a pure solvent cast PEO:LiTFSI (20:1) electrolyte membrane. At 80°C, the optimised printed electrolyte does not create short circuits upon cycling, unlike pure PEO-LiTFSI reference membrane. PP highly improves the mechanical stability of the electrolyte: the pure PEO-LiTFSI membrane loses up to 98% of its initial thickness against less than 30% for the printed electrolyte under 6N and 100°C for 30 min. Thus, a ring of mylar was used to avoid creeping the pure PEO:LiTFSI electrolyte as mentioned in the setup (Figure S13 of the supplementary material). Cycling results of LFP/Li° cells showcase a higher polarisation for the printed samples than the reference membrane (140 mV/190 mV against 50 mV) (Figure 8a). This can be explained by a lower ionic conductivity and a lower thickness loss for the printed electrolytes. Despite the gap of ionic conductivities for the printed SPE at 40°C and 80°C, differences in polarisation between 80°C and 40°C have been limited by the use of adapted areal capacities at each temperature. For both temperatures, a decrease in discharge capacity at C/5 is visible but the initial capacity comes back at C/20 (Figure 8b). This shows that the capacity loss is not linked to irreversible degradations. It can come from too high current densities at C/5 that increase the polarisation, combined with the absence of lithium salt in the polymer cathode formulation. Capacities are lower at 40°C than those obtained at 80°C for the same reasons.

Conclusion

This work reports a novel solvent-free polymer electrolyte, achieved by FFF 3D printing in a view to in-space 3D printing of Li-ion batteries. The mechanical properties of a PEO + LiTFSI-based conductive electrolyte were strengthened by adding an immiscible polymer phase of PP via a full solvent-free extrusion process. A fine-tuning of the PEO/LiTFSI viscosity and crystallinity has been performed by studying the influence of three parameters: PP content, LiTFSI content, and PEO molar weight. Thanks to this, a co-continuous morphology has been obtained to maximise the ionic conductivity and the 3D printability by FFF. The best formulation with 40 wt% of PP, O/Li^+ = 10:1, and a mix of two PEO with different molar weights, has been successfully 3D printed on a commercial printer. This 200 µm thick disk displays the highest ionic conductivity reported so far for polymer electrolyte 3D printed in one shot by FFF with 1.5×10^{-5} S.cm^{-1} at 30°C. The ionic conductivity is higher than that of a classical PEO/LiTFSI at 30°C but still lower than that of a classical system at T°C > 50°C. The 3D-printed electrolyte has been successfully cycled in an LFP/Li^0 metal coin cell at 80°C (1.04 mAh/cm^2) and 40°C (0.53 mAh/cm^2). PP brings mechanical stability that limits the creeping and avoids short circuits compared to a pure PEO/LiTFSI electrolyte. LFP/Li^0 metal cells offer encouraging performances that still could be improved because the ionic conductivity (1.5×10^{-5} S.cm^{-1} at 30°C) and the thickness (200 µm) of printed electrolyte lead to polarisation that impacts cycling performances at a high C rate. Nonetheless, this one-shot printed electrolyte opens the way towards replacing the printed separator to 3D print the entire Li-ion battery without any post-treatment. In the case of full-cell printing, electrolyte layer thickness can be decreased up to 100 µm, and an optimised 3D architecture can increase the area-to-volume ratio resulting in improved electrochemical performances. Composite polymer electrolyte seems to be a promising answer to enhance the ionic conductivity for low-temperature applications. Ceramic particles can bring mechanical reinforcement and disturb the crystallinity to reduce the need for high molar weight PEO or PP. It could also increase conductive phase viscosity to reach co-continuity with a lower content of PP, and it could

offer a new pathway for Li^+ in the case of ionic conductive particle addition.

Acknowledgment

The authors would like to thank Raynald Lesieur, Victor Boudeville, Sebastian Ursescu, Stéphane Panier, and Michel Armand either for technical support or fruitful scientific discussions that contributed to this project.

Disclosure statement

No potential conflict of interest was reported by the author(s).

Funding

This work was supported by the Région Hauts-de-France, the European Space Agency (ESA), and the University of Picardie Jules Verne (UPJV). It was performed in the frame of ESA Contract 4000139673.

Data availability statement

The data that support the findings of this study are available from the corresponding author, [LD], upon reasonable request.

References

[1] Creech S, Guidi J, Elburn D. Artemis: an overview of NASA's activities to return humans to the moon. 2022 IEEE Aerospace Conference (AERO); 2022. p. 1–7.
[2] NASA'S management of the Artemis missions – November 15, 2021.
[3] Makaya A, Pambaguian L, Ghidni T, et al. Towards out of earth manufacturing: overview of the ESA materials and processes activities on manufacturing in space. CEAS Space J. 2022;15:69–75.
[4] Owens A, De Weck O. Systems analysis of in-space manufacturing applications for the international space station and the evolvable Mars campaign. In: AIAA SPACE; 2016 Sep 13–16; Long Beach, CA. AIAA SPACE Forum(AIAA 2016-5394); 2016.
[5] Musso G, Lentini G, Enrietti L, et al. Portable on orbit printer 3D: 1st European additive manufacturing machine on international space station. In: Goonetilleke R, Karwowski W, editors. Advances in physical ergonomics and human factors; Florida, USA. Cham: Springer; 2016, p. 643–655.
[6] Prater T, Werkheiser N, Ledbetter F, et al. 3D printing in Zero G Technology Demonstration Mission: complete experimental results and summary of related material modeling efforts. Int J Adv Manuf Technol. 2019;101(1-4):391–417. doi:10.1007/s00170-018-2827-7
[7] Zhang F, Wei M, Viswanathan VV, et al. 3D printing technologies for electrochemical energy storage. Nano Energy. 2017;40:418–431.
[8] Ambrosi A, Pumera M. 3D-printing technologies for electrochemical applications. Chem Soc Rev. 2016;45(10):2740–2755.
[9] Lyu Z, Lim GJH, Koh JJ, et al. Design and manufacture of 3D-printed batteries. Joule. 2021;5(1):89–114.
[10] Wang J, Sun Q, Gao X, et al. Toward high areal energy and power density electrode for Li-Ion batteries via optimized 3D printing approach. ACS Appl Mater Interfaces. 2018;10(46):39794–39801.
[11] Cai J, Fan Z, Jin J, et al. Expediting the electrochemical kinetics of 3D-printed sulfur cathodes for Li–S batteries with high rate capability and areal capacity. Nano Energy. 2020;75:104970, doi:10.1016/j.nanoen.2020.104970
[12] Cardenas JA, Bullivant JP, Kolesnichenko IV, et al. 3D printing of ridged FeS2 cathodes for improved rate capability and custom-form lithium batteries. ACS Appl Mater Interfaces. 2022;14(40):45342–45351.
[13] Huifa S, Jiakai C, Zhenhua S, et al. 3DPrinting enables customizable batteries. Batteries Supercaps. 2023;6(7).
[14] Goh GL, Zhang H, Chong TH, et al. 3D printing of multilayered and multimaterial electronics: a review. Adv Electron Mater. 2021;7(10):2100445, doi:10.1002/aelm.202100445
[15] Maurel A, Grugeon S, Armand M, et al. Overview on Lithium-Ion battery 3D-printing by means of material extrusion. ECS Trans. 2020;98(13):3.
[16] Foster CW, Zou GQ, Jiang Y, et al. Next-generation additive manufacturing: tailorable graphene/polylactic(acid) filaments allow the fabrication of 3D printable porous anodes for utilisation within lithium-Ion batteries. Batteries Supercaps. 2019;2(5):448–453. doi:10.1002/batt.201800148
[17] Reyes C, Somogyi R, Niu S, et al. Three-dimensional printing of a complete Lithium Ion battery with fused filament fabrication. ACS Appl Energy Mater. 2018;1(10):5268–5279.
[18] Maurel A, Courty M, Fleutot B, et al. Highly loaded graphite–polylactic acid composite-based filaments for Lithium-Ion battery three-dimensional printing. Chem Mater. 2018;30(21):7484–7493.
[19] Boudeville V, Grugeon S, Maurel A, et al. Solvent-free extrusion of a LiFePO4-based monofilament for three-dimensional printing of a lithium-ion battery positive electrode. J Power Sources. 2024;593:233973, doi:10.1016/j.jpowsour.2023.233973
[20] Maurel A, Armand M, Grugeon S, et al. Poly(ethylene oxide)−LiTFSI solid polymer electrolyte filaments for fused deposition modeling three-dimensional printing. J Electrochem Soc. 2020;167:070536.
[21] Meng N, Lian F, Cui G. Macromolecular design of lithium conductive polymer as electrolyte for solid-state lithium batteries. Small. 2021;17(3):2005762.
[22] Xue Z, He D, Xie X. Poly(ethylene oxide) – based electrolytes for lithium-ion batteries. J Mater Chem A. 2015;3:19218.
[23] Ragones H, Vinegrad A, Ardel G, et al. On the road to a multi-coaxial-cable battery: development of a novel 3D-printed composite solid electrolyte. J Electrochem Soc. 2019;167(7):070503.
[24] Vinegrad A, Ragones H, Jayakody N, et al. Plasticized 3D-printed polymer electrolytes for Lithium-Ion batteries. J Electrochem Soc. 2021;168(11):110549.
[25] Bourseau F, Grugeon S, Lafont U, et al. 3D printing of solid polymer electrolytes by fused filament fabrication:

challenges towards in-space manufacturing. J Phys Energy. 2023;6(1):012001.
[26] Pötschke P, Paul DR. Formation of co-continuous - structures in melt-mixed immiscible polymer blends. J Macromol Sci Part C: Polym Rev. 2003;43 (1):87–141.
[27] Zheng F, Li C, Li Z, et al. Advanced composite solid electrolytes for lithium batteries: filler dimensional design and Ion path optimization. Small. 2023;19(21):2206355.
[28] Zhuang H, Ma W, Xie J, et al. Solvent-free synthesis of PEO/garnet composite electrolyte for highsafety all-solid-state lithium batteries. J Alloys Compd. 2020;860:157915.
[29] Bouchet R, Phan TNT, Devaux D, et al. Charge transport in nanostructured PS-PEO-PS triblock copolymer electrolytes. Macromolecules. 2014;47:2659–2665. doi:10.1021/ma500420w
[30] Hallinan DT, Balsara NP. Polymer electrolytes. Annu Rev Mater Res. 2013;43(1):503–525.